Perovskite-Si solar cell: A three-terminal heterojunction bipolar transistor architecture

Perovskite-Si solar cell: a three-terminal heterojunction bipolar transistor architecture

Gemma Giliberti
Department of Electronics and Telecommunications
Politecnico di Torino
Torino, Italy
gemma.giliberti@polito.it

Antonio Martí
Instituto de Energía Solar
Universidad Politécnica de Madrid
Madrid, Spain
antonio.marti@upm.es

Federica Cappelluti
Department of Electronics and Telecommunications
Politecnico di Torino
Torino, Italy
federica.cappelluti@polito.it

***Abstract*—Over the past decade, perovskite materials have attracted great interest for terrestrial photovoltaic (PV) applications thanks to their cheapness and excellent optoelectronic properties such as tunable bandgap, high absorption coefficient, long carrier lifetime and diffusion length. Perovskites have excellent potential for the development of high efficiency and low cost silicon-based tandem solar cells. Several research studies have been performed about perovskite/silicon tandem solar cells obtaining good conversion efficiencies of about 26%. In this work, we propose a perovksite-silicon solar cell based on the three-terminal hetero-junction bipolar transistor (3T-HBJT) architecture that overcomes several constraints of the series connected double junction cell - i.e. current matching and the need of tunnel junctions or recombination layers - exploiting a simpler structure and achieving high efficiency. In order to evaluate its performance potential, we adopt the classical Hovel model extended to deal with the 3T-HBT structure, demonstrating efficiencies up to 28.6% for cells without antireflection coating.**

I. Introduction

The energy demand increases exponentially and is expected to do so in the years ahead. Until now, fossil fuels are the most exploited non-renewable sources of energy responsible for climate change and global warming. In this scenario, photovoltaic technology represents a viable alternative blending cheapness and sustainability. Nowadays, the terrestrial PV market is dominated by c-Si single-junction (SJ) solar cells achieving efficiency of $\sim$26.6% [1] close to their theoretical limit of $\sim$ 29%. A good way to overcome this limit is exploiting tandem solar cells stacking different materials that harvest a wide spectral range of the solar spectrum thanks to their different band-gaps. III-V semiconductors tandem cells are by far the highest efficiency technology but their manufacturing costs are still too high to enter in the terrestrial PV market. On the other hand, finding a suitable widegap material to realize silicon tandems is not obvious. In the last years, a possible solution is found in organic-inorganic lead halide perovskite (PVK), firstly proposed by Miyasaka et al. [2]. Although many shortcomings of PVK material such as degradation under ultraviolet radiation and toxicity linked to the presence of lead (Pb) have not yet been solved, low manufacturing costs as well as strong solar absorption and high carrier lifetime make it an attractive potential top-cell for Si-based tandems. In 2018, Sahli et al., [3] proposed a fully textured PVK-Si tandem solar cell with an efficiency of $\sim$ 25.2% and also a certified record of $\sim$ 27.3% was achieved [4]. More recently, an efficiency of $\sim$ 26.0% has been demonstrated by Eike Köhnen at al., by reducing the current mismatch between the sub-cells [5].

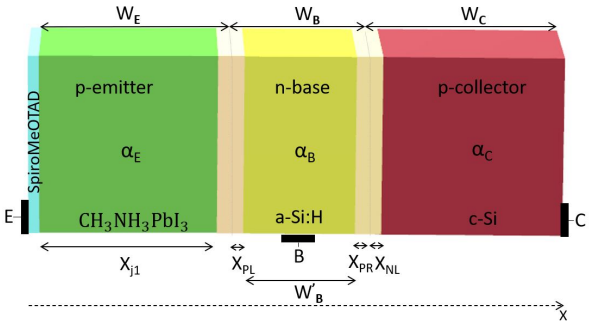

Fig. 1. Structure of the proposed three-terminal HBT-SC: SpiroMeOTAD layer as hole trasport material, p-doped PVK emitter, n-doped a-Si:H base, and p-doped c-Si collector.

In this work, with the aim of further increasing the PVK/Si solar efficiency and at the same time reducing the complexity of the structure, we exploit an alternative architecture: the three-terminal hetero-junction bipolar transistor solar cell (3T-HBTSC) [6] shown in Fig. 1. It consists of a hole transport SpriroMeOTAD layer (HTM), a p-doped PVK emitter, a n-doped a-Si:H base, and a p-doped c-Si collector. It is possible to identify emitter/base (E/B) and base/collector (B/C) sub-cells equivalent to the top and bottom sub-cells of a double-junction (DJ) architecture, but electrically connected through the common base layer. Although the presence of three metal contacts is a tricky point for fabrication and design optimization, this kind of architecture offers the possibility to overcome the current matching constraints avoiding also the tunnel junctions, and achieving the same efficiency of DJ cells through proper optimization. In order to evaluate the cell performance and quantify the total efficiency, optoelectronic simulations of the PVK/Si 3T-HBTSC are carried out on the basis of the well established Hovel model [7] properly extended to the p-n-p heterostructure [8]. This allows to assess the cell behavior based on accurate and reliable material

parameters, obtaining a realistic estimation of the achievable efficiency.

II. Analytical approach

The Hovel model is extended to the p-n-p (n-p-n) heterostructure obtaining an analytical solution to the drift-diffusion problem. Treating the HTM similarly to a window layer, we have considered in the emitter, base and collector layers, the continuity equation for minority carriers under low-injection condition and quasi-neutrality approximation. We summarize here the most relevant equations, while the complete model formulation will be reported elsewhere [8].

The diffusion equation for minority holes, p_n, in the quasi-neutral base region reads as

$$\frac{d^2(p_n - p_{n0})}{dx^2} = \frac{p_n - p_{n0}}{D_p \tau_p} - \frac{G\mathrm{e}^{-\alpha_\mathrm{B}(x-W_\mathrm{E})}}{D_p} \qquad (1)$$

where $G = (1-R_\mathrm{E})(1-R_\mathrm{B})\alpha_\mathrm{B}\mathrm{e}^{(-\alpha_\mathrm{E}W_\mathrm{E})}\Phi$. $R_{\mathrm{E(B)}}$ is the reflectance at the emitter-window (base-emitter) interface, $\alpha_{\mathrm{E(B)}}$ and $W_{\mathrm{E(B)}}$ are the optical absorption and thickness of the emitter (base) layer, respectively, p_{n0} is the hole minority carrier density under thermodynamic equilibrium, D_p is the diffusion coefficient, τ_p is the hole lifetime, and Φ is the photon flux.

Eq.1 can be solved under two boundary conditions identified by the junction law

$$p_n(x^*) - p_{n0} = p_{n0}\left(\mathrm{e}^{qV^*/k_\mathrm{B}T} - 1\right) \qquad (2)$$

with $V^* = V_\mathrm{EB}$ for $x^* = W_\mathrm{E} + x_\mathrm{PL}$, and $V^* = V_\mathrm{CB}$ for $x^* = W_\mathrm{E} + W_\mathrm{B} - x_\mathrm{PR}$, $x_{\mathrm{PL(PR)}}$, $x_{\mathrm{PL(PR)}}$ being the thickness of the depleted base region at the E/B and C/B junctions, respectively (see Fig. 1). Photocurrent generation in the depleted regions is taken into account assuming unitary collection efficiency. Once Eq. 1 is solved, we obtain the total base current $Jp^\mathrm{B}(\Phi, V_\mathrm{EB}, V_\mathrm{CB})$ whose dark current component depends on both E/B and B/C self-bias voltages, so that the two sub-cells are not completely independent each other. The generated electrical power is extracted from two independent loads connected between E/B and B/C metal contacts.

TABLE I
Main parameter values [5] [9] [10] [11] [12].

	$CH_3NH_3PbI_3$ p-emitter	a-Si:H n-base	c-Si p-collector
Thickness [nm]	350	600	2×10^5
Eg [eV]	1.55÷1.6	1.7	1.1
Doping [cm^{-3}]	10^{16}	3×10^{18}	10^{16}
ni [cm^{-3}]	$8 \times 10^4 \div 3.8 \times 10^5$	9×10^4	9.6×10^9
Mobility [$\mathrm{cm}^2/\mathrm{Vs}$]	$11.8^{[e]}$	$5^{[h]}$	$1177^{[e]}$
Electron affinity [eV]	3.73	3.9	4.05
B [$\mathrm{cm}^3 s^{-1}$]	$8 \times 10^{-10} \div 10^{-9}$	1.8×10^{-15}	1.1×10^{-14}
τ_{rad}	97÷125 ns	0.15 ms	9 ms
τ_{SRH}	736 ns	-	1 ms
τ_{tot}	85÷106 ns	100 ns	0.9 ms

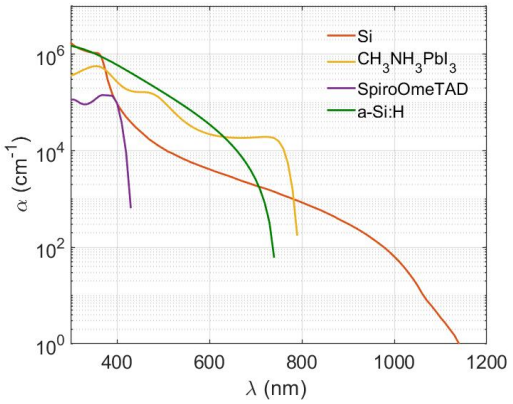

Fig. 2. Absorption coefficient (α) of the materials used in this work [13], [14], [15]

III. Materials

A proper selection of materials for emitter, base and collector is a crucial step in order to provide a high photon collection. With this aim, we have chosen for the emitter layer a PVK material with certain characteristics. Materials used in this study and their main parameters are summarized in Table 1. Perovskites are described by the formula ABX_3: A and B are cations of different sizes, instead X is an anion. For PV applications, organic-inorganic halide PVKs ($CH_3NH_3PbX_3$ where X=Cl, Br and I) are exploited using the methylammonium ($CH_3NH_3^+$) and Pb respectively for the cations A and B, while a halogen such as I, Br or Cl is used for the anion X. Based on the halogen, both electrical and optical properties change, affecting solar cell efficiency. From simulations, it results that in order to maximize the solar cell efficiency, it is convenient to choose the methylammonium lead triiodide ($CH_3NH_3PbI_3$) that shows the lowest energy gap, $E_\mathrm{g} = 1.55 \div 1.6$ eV, covering the entire visible region ($\lambda < 800$ nm), and has the highest absorption coefficient [13] (Fig. 2). For this case study, we consider a doping concentration of $\sim 10^{16}\mathrm{cm}^{-3}$ [10] as reported in Table I. The table summarizes also a range of values used in the simulations for intrinsic carrier density [5] [10], energy gap [5] [10], radiative recombination coefficient (B) [5] [12], since these are affected by the PVK fabrication process. In order to extract carriers efficiently from the p-emitter is necessary to consider a hole transport material such as spiro-OMeTAD [16] between the emitter contact and the PVK layer. For the base region, several simulations were carried out exploiting Hydrogenated Amorphous Silicon Carbon $a-Si_{1-x}C_x : H$ that has a tunable bandgap according to the x molar fraction

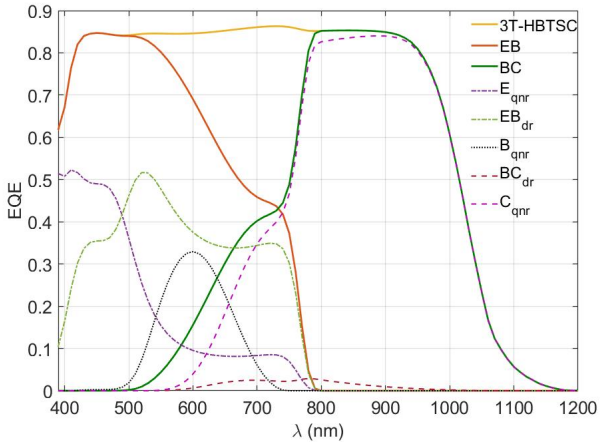

Fig. 3. External quantum efficiency of the 3T-HBTSC (yellow line) and of the sub-cells components (dashed lines), including quasi neutral regions (qnr) and depleted regions (dr).

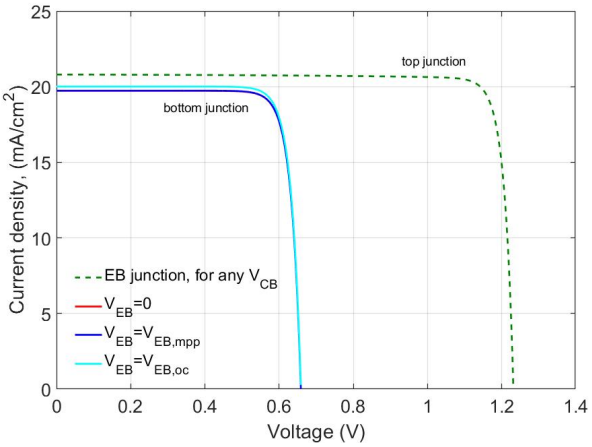

Fig. 4. Current-voltage characteristics of the emitter-base and base-collector junctions at different V_{CB} and V_{EB}, respectively.

[14]. The best efficiency is achieved for a molar fraction $x = 0$ i.e. Hydrogenated Amorphous Silicon ($a - Si : H$) having an energy gap of $\sim$ 1.7 eV. Since the base has higher E_g than that one of the emitter, the formed heterojunction allows to increase the E/B open circuit voltage with respect to the PVK homojunction case. Finally, crystalline silicon (c-Si) is used for the collector layer that harvests the rest of the solar spectrum. Simulations consider both radiative and nonradiative recombination, according to the lifetime constants reported in Table I.

IV. Results

Fig. 3 shows the External Quantum Efficiency (EQE) of the 3T-HBTSC and the partial contributions from emitter, base and collector quasi-neutral and depleted regions. The device is simulated without anti-reflection layer, hence the total EQE shows a significant penalty due to the air-window reflectance. Most photons, absorbed in the emitter layer, generate e-h pairs close to the surface since the direct bandgap $CH_3NH_3PbI_3$ material has strong absorption at short wavelengths (Fig.2). Although the base layer has energy gap higher than that one of the emitter, it absorbs part of the solar spectrum contributing to the total amount of photogenerated current, because the emitter is thin ($W_E \sim 350$ nm) and a certain fraction of long wavelength photons are not absorbed and escape towards the base and collector layers.

Fig. 4 shows the E/B and B/C current voltage characteristics. For the structure/materials under study we observe that carrier injection from one junction to the other is almost negligible in any operating condition, i.e. the transistor effect is suppressed. In fact, the injection from B/C to E/B is totally negligible owing to the higher E/B open-circuit voltage with respect to that one of the B/C junction. Moreover, also carrier injection from E/B to B/C is marginal for any value of V_{EB}.

Therefore, the 3T-HBTSC efficiency can be estimated studying the two junctions as if they were independent. The calculated photovoltaic parameters are reported in Table 2. The cell achieves a total efficiency ranging between $\sim$ 27.1% and 28.6%, depending on the assumed values for radiative recombination coefficient and intrinsic carrier density of the PVK layer, in line with those reported in [3] [5] for DJ architectures. Reducing the optical losses, the device can overcome the threshold of $\sim$30%.

TABLE II
Performance of the 3T-HBTSC.

Total efficiency 27.1÷28.6%	Voc [V]	Jsc [mA/cm^2]	Vmpp [V]	Jmpp [mA/cm^2]	FF [%]	η [%]
Emitter-Base $V_{CB} = 0$	1.17 ÷ 1.25	20.8	1.05 ÷ 1.13	20.1	86.6 ÷ 87.4	17.9÷ 19.4
Collector-Base $V_{EB} = 0$	0.66	19.7	0.58	18.8	83.9	9.2

Acknowledgments

A.M acknowledges Project GRECO (787289 H2020 Grant Agreement), funded by the European Commission.

References

[1] K. Yoshikawa, W. Yoshida, T. Irie, H. Kawasaki, K. Konishi, H. Ishibashi, T. Asatani, D. Adachi, M. Kanematsu, H. Uzu, and K. Yamamoto, "Exceeding conversion efficiency of 26heterojunction interdigitated back contact solar cell with thin film si technology," *Solar Energy Materials and Solar Cells*, vol. 173, pp. 37–42, 2017.

[2] A. Kojima, K. Teshima, Y. Shirai, and T. Miyasaka, "Organometal halide perovskites as visible-light sensitizers for photovoltaic cells," *Journal of the American Chemical Society*, vol. 131, no. 17, p. 6050, 2009.

[3] F. Sahli, J. Werner, B. A. Kamino, M. Bräuninger, R. Monnard, B. Paviet-Salomon, L. Barraud, L. Ding, J. J. Diaz Leon, D. Sacchetto, G. Cattaneo, M. Despeisse, M. Boccard, S. Nicolay, Q. Jeangros, B. Niesen, and C. Ballif, "Fully textured monolithic perovskite/silicon tandem solar cells with 25.2efficiency," *Nature materials*, vol. 17, no. 9, p. 820, 2018.

[4] M. A. Green, E. D. Dunlop, D. H. Levi, J. Hohl-Ebinger, M. Yoshita, and A. W. Y. Ho-Baillie, "Solar cell efficiency tables (version 54," *Progress in Photovoltaics: Research and Applications*, vol. 27, no. 7, pp. 565–575, 2019.

[5] E. Khnen, M. Jot, A. B. Morales-Vilches, P. Tockhorn, A. Al-Ashouri, B. Macco, L. Kegelmann, L. Korte, B. Rech, R. Schlatmann, B. Stannowski, and S. Albrecht, "Highly efficient monolithic perovskite silicon tandem solar cells: analyzing the influence of current mismatch on device performance," *Sustainable Energy & Fuels*, vol. 3, no. 8, pp. 1995–2005, 2019.

[6] A. Martí and A. Luque, "Three-terminal heterojunction bipolar transistor solar cell for high-efficiency photovoltaic conversion," *Nature communications*, vol. 6, no. 1, pp. 1–6, 2015.

[7] H. J. Hovel, *Semiconductors and semimetals. Volume 11. Solar cells*. Academic Press, Inc., New York, 1975.

[8] G. Giliberti and *et al.*, *in preparation*, 2020.

[9] H. Imran, I. Durrani, M. Kamran, T. M. Abdolkader, M. Faryad, and N. Z. Butt, "High-performance bifacial perovskite/silicon double-tandem solar cell," *IEEE Journal of Photovoltaics*, vol. 8, no. 5, pp. 1222–1229, 2018.

[10] B. Olyaeefar, S. Ahmadi-Kandjani, and A. Asgari, "Bulk and interface recombination in planar lead halide perovskite solar cells: A drift-diffusion study," *Physica E: Low-dimensional Systems and Nanostructures*, vol. 94, pp. 118–122, 2017.

[11] T. Kirchartz, F. Staub, and U. Rau, "Impact of photon recycling on the open-circuit voltage of metal halide perovskite solar cells," *ACS Energy Letters*, vol. 1, no. 4, pp. 731–739, 2016.

[12] Y. Zhou and A. Gray-Weale, "A numerical model for charge transport and energy conversion of perovskite solar cells," *Phys. Chem. Chem. Phys.*, vol. 18, pp. 4476–4486, 2016. [Online]. Available: http://dx.doi.org/10.1039/C5CP05371D

[13] M. Shirayama, H. Kadowaki, T. Miyadera, T. Sugita, M. Tamakoshi, M. Kato, T. Fujiseki, D. Murata, S. Hara, T. N. Murakami, S. Fujimoto, M. Chikamatsu, and H. Fujiwara, "Optical transitions in hybrid perovskite solar cells: Ellipsometry, density functional theory, and quantum efficiency analyses for ch 3 nh 3 pbi 3," *Physical Review Applied*, vol. 5, no. 1, 2016.

[14] D. K. Basa, G. Abbate, G. Ambrosone, U. Coscia, and A. Marino, "Spectroscopic ellipsometry study of hydrogenated amorphous silicon carbon alloy films deposited by plasma enhanced chemical vapor deposition," *Journal of Applied Physics*, vol. 107, no. 2, 2010.

[15] M. A. Green, "Self-consistent optical parameters of intrinsic silicon at 300 k including temperature coefficients," *Solar Energy Materials and Solar Cells*, vol. 92, no. 11, pp. 1305–1310, 2008.

[16] M. Jošt, L. Kegelmann, L. Korte, and S. Albrecht, "Monolithic perovskite tandem solar cells: A review of the present status and advanced characterization methods toward 30% efficiency," *Advanced Energy Materials*, vol. n/a, no. n/a, p. 1904102, 2019. [Online]. Available: https://onlinelibrary.wiley.com/doi/abs/10.1002/aenm.201904102